Direct Observation of Coherent Longitudinal and Shear Acoustic Phonons in TaAs Using Ultrafast X-Ray Diffraction

Min-Cheol Lee, N. Sirica, S. W. Teitelbaum, A. A Maznev, Thomas Pezeril, R. Tutchton, V. Krapivin, G. A. de La Pena, Y. Huang, L. X. Zhao, et al.

Direct Observation of Coherent Longitudinal and Shear Acoustic Phonons in the Weyl Semimetal TaAs Using Ultrafast X-ray Diffraction

M. -C. Lee, N. Sirica, S. W. Teitelbaum, A. Maznev, Thomas Pezeril, R. Tutchton, V. Krapivin, G. A. de La Pena, Y. Huang, L. X. Zhao, et al.

Direct Observation of Coherent Longitudinal and Shear Acoustic Phonons in the Weyl Semimetal TaAs Using Ultrafast X-ray Diffraction

Min-Cheol Lee,[1,*] N. Sirica,[1] S. W. Teitelbaum,[2,3] A. Maznev,[4,5] T. Pezeril,[4,6] R. Tutchton,[1] V. Krapivin,[2,3,7] G. A. de la Pena,[2,3] Y. Huang,[2,3,7] L. X. Zhao,[8] G. F. Chen,[8] B. Xu,[8] R. Yang,[8] J. Shi,[4] J.-X. Zhu,[1] D. A. Yarotski,[1] X. G. Qiu,[8] K. A. Nelson,[4,5] M. Trigo,[2,3] D. A. Reis,[2,3,7,9] and R. P. Prasankumar[1,†]

[1] *Center for Integrated Nanotechnologies, Los Alamos National Laboratory, Los Alamos, New Mexico 87545, USA*
[2] *Stanford PULSE Institute, SLAC National Accelerator Laboratory, Menlo Park, California 94025, USA*
[3] *Stanford Institute for Materials and Energy Sciences, SLAC National Accelerator Laboratory, Menlo Park, California 94025, USA*
[4] *Department of Chemistry, Massachusetts Institute of Technology, 77 Massachusetts Avenue, Cambridge, MA, 02139, USA*
[5] *Institute for Soldier Nanotechnology, Massachusetts Institute of Technology, 500 Technology Square, NE47-598, Cambridge, MA, 02139, USA*
[6] *Institut de Physique de Rennes, Université de Rennes 1, UMR CNRS 6251, 35000 Rennes, France*
[7] *Department of Applied Physics, Stanford University, Stanford, California 94305, USA*
[8] *Institute of Physics, Chinese Academy of Sciences, Beijing 100190, China*
[9] *Department of Photon Science, Stanford University, Stanford, California 94305, USA*

(Dated: November 17, 2020)

Using femtosecond time-resolved X-ray diffraction, we investigate optically excited coherent acoustic phonons in the Weyl semimetal TaAs. The low symmetry of the (112) surface probed in our experiment enables the simultaneous excitation of longitudinal and shear acoustic modes, whose dispersion closely matches first-principles calculations and previously measured elastic properties. We find an asymmetry in the spectral lineshape of the longitudinal mode that is notably absent from the shear mode, suggesting a time-dependent frequency chirp that is likely driven by photoinduced carrier diffusion. Our study underscores the benefit of using off-axis crystal orientations when optically exciting shear deformations in topological semimetals, allowing one to transiently change their crystal structure and potentially their topological properties.

Ultrafast spectroscopy is a powerful tool for studying structural dynamics in quantum materials through the generation of coherent phonon oscillations driven by femtosecond optical pulses [1–4]. The coherent excitation of acoustic phonons occurs when an intense femtosecond optical pump pulse launches a strain wave along the surface normal, resulting from, for example, thermoelastic, electron-phonon coupling, and piezoelectric effects that are driven by the photoexcitation of charge carriers [4–9]. This optically induced strain wave is then measured in the time domain via coherent oscillations in the reflectivity or transmission of an additional optical probe pulse, when the probe penetrates deeper than the acoustic wavelength. Optical pump-probe spectroscopy has thus been used to observe longitudinal acoustic phonons with gigahertz (GHz) to terahertz (THz) frequencies in a wide range of materials [10]. In contrast, the generation of transverse acoustic (shear) modes is less common, as it requires a specific choice of crystal geometry [5, 6]. However, the ability to optically excite these modes could provide a unique opportunity for tuning both symmetry and topology in quantum materials [11–13].

Recently, the advent of ultrafast X-ray free-electron lasers (XFELs) has led to significant advances in the study of structural dynamics, making it possible to directly probe the generation of coherent phonons following optical excitation [8, 14–16], even at high (THz) frequencies [16], without requiring the superlattice structures used previously [17–20]. In this paper, we leverage these recent developments in ultrafast X-ray spectroscopy to directly track coherent acoustic phonons in the Weyl semimetal TaAs following femtosecond optical excitation. Time-resolved X-ray diffraction (tr-XRD) was used to probe real-time oscillations in the crystal truncation rod, which arises from the structural boundary imposed by the crystal surface [8, 21, 22]. Due to the distinct crystallographic orientation of the (112) face probed in our experiments, we simultaneously observed both longitudinal and shear acoustic phonon modes. Our data reveals a positive frequency chirp in the longitudinal mode that is absent from the shear mode. This has not previously been observed in any material via tr-XRD, to the best of our knowledge, and is likely due to phonon softening via ambipolar diffusion of photoinduced carriers. These first ultrafast XRD experiments on topological semimetals thus demonstrate the power of this technique for providing new insight into structural dynamics in these systems.

We performed optical-pump, X-ray-probe measurements at the X-ray pump-probe (XPP) instrument [8] of the Linac Coherent Light Source (LCLS) XFEL [14]. Fig. 1(a) shows a schematic of the experimental geometry, where photoinduced changes in a (112) oriented TaAs single crystal driven by 800 nm (1.55 eV) optical pump pulses (incident fluence = 2.86 mJ/cm^2) were probed by monochromatic X-ray pulses at a 120 Hz repetition rate,

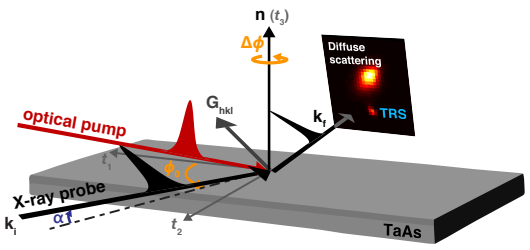

FIG. 1. Schematic diagram of the time-resolved X-ray diffraction experiment, including the crystal truncation rod scattering (TRS) signal, performed on the (112) face of TaAs.

centered at 9.52 keV. We operated in a reflection geometry with the X-ray probe (optical pump) projected onto the sample at a grazing angle of $\alpha = 3°$ (5.3°), giving penetration depths of 500 nm (22 nm). Transient changes in the X-ray scattering intensity were measured with an area detector [23]. The temporal duration of both optical pump and X-ray probe pulses was below 80 fs.

The X-ray scattering signal was measured along the (103)-q(112) truncation rod, where q defines the wave vector parallel to the (112) surface normal of our TaAs single crystal; importantly, this enabled us to directly measure changes in the local lattice spacing along the surface normal. Detection of the (103) Bragg peak was accomplished by satisfying the Laue condition $\vec{G}_{hkl} = \vec{k}_f - \vec{k}_i$, in which $\vec{G}_{hkl}$ defines the reciprocal lattice vector for the body centered tetragonal ($I4_{1md}$) space group of TaAs [24, 25], while $\vec{k}_i$ ($\vec{k}_f$) defines the wavevector for the incident (diffracted) X-ray beam, as shown in Fig. 1. Due to the presence of a finite surface boundary in real space, truncation rod scattering (TRS) arises between Bragg points [26]; our experiment follows the truncation rod from the (103) to the (0$\bar{1}$1) Bragg peaks [27].

By varying the azimuthal angle by $\Delta\phi$ about the surface normal, the scattering condition is modified to $\vec{k}_f - \vec{k}_i = \vec{G}_{hkl} + \vec{q}$, which enables us to directly probe the generation of coherent phonons in the TRS signal with a momentum $\vec{q} = q\hat{n}$ along the surface normal. This is a significant advantage over coherent phonon observations with optical probes, which are only sensitive to the entire phonon spectrum near zone-center. This azimuthal sample rotation ensures that the incident angle, α, remains fixed, as is necessary to maintain a constant X-ray penetration depth at grazing incidence. As shown in the supplemental material, the phonon momentum q can then be determined by $\Delta\phi$ and the geometric relation [27],

$$q = \Delta\phi G_{hkl} k \cos\alpha \frac{\sin\phi_0 \cos\theta_1 - \cos\phi_0 \cos\theta_2}{G_{hkl}\cos\theta_3 - k\sin\alpha}, \quad (1)$$

where $k = |k_i| = |k_f|$, ϕ_0 is the azimuthal angle that satisfies the Laue condition for the (103) Bragg peak, and $\vec{G}_{hkl} = G(\cos\theta_1, \cos\theta_2, \cos\theta_3)$ defines the reciprocal lattice vector in terms of directional cosines with respect to the Cartesian coordinates (t_1, t_2, t_3) (Fig. 1) [27].

Fig. 2(a-c) depicts two-dimensional images from our tr-XRD experiments, showing both diffuse scattering and TRS signals. Here, the separation between these two features grows as the azimuthal angle deviates from ϕ_0 by $\Delta\phi$. From Eq. (1), this corresponds to an increase in coherent phonon momentum q, leading to higher oscillation frequencies for acoustic phonon modes. Fig. 2(d-f) shows transient changes to the TRS signal probed by tr-XRD. These traces ($I_{\text{norm}}(t)$) are obtained by integrating the diffraction intensity over a small 3×3 pixels area ($0.36° \times 0.36°$) region of the detector (indicated by the blue arrows in Fig. 2(a-c)) and normalizing to the equilibrium intensity measured prior to pump excitation ($t < 0$). We find that $I_{\text{norm}}(t)$ exhibits clear oscillations at sub-terahertz frequencies that scale with increasing q, characteristic of coherent acoustic phonons generated by femtosecond photoexcitation [16, 21].

To extract the relevant oscillatory and decay parameters, we fit our data in Fig. 2(d-f) with the convolution of a Gaussian instrumental response, which captures the 80 fs time resolution of our experiment, and a phenomenological function, $g(t)$, composed of a single exponential decay and two damped oscillatory components:

$$g(t) = A_l e^{-t/\tau_l} + \sum_{i=1,2} A_i e^{-t/\tau_i} \cos(2\pi f_i t - \varphi_i) \quad (2)$$

The time constants τ_l and τ_i represent a decay due to lattice cooling and the dephasing times for coherent phonon oscillations, respectively. Similarly, A_l represents the amplitude of the slow dynamics, and A_i, f_i and φ_i denote the respective amplitude, frequency, and initial phase for the oscillations.

Using Eq. (2) to fit to the transient TRS signal for different values of $\Delta\phi$ reveals the presence of multiple frequency components. In Fig. 2(g-i), we isolate these frequency components by subtracting the effect of lattice cooling (i.e., the first term in Eq. (2)) from the overall transients. Fourier transforms of the coherent phonon oscillations clearly show two distinct frequencies, as shown in Fig. 2(k-l). This observation of multiple coherent phonon modes in tr-XRD measurements is surprising, as previous experiments on other materials have predominantly revealed a single longitudinal acoustic mode traveling along the surface normal [16, 21, 22]. This is due to the fact that shear deformations are not generated under photoexcitation when the surface plane is isotropic, as the transverse lattice displacements that accompany shear wave generation require broken symmetry [5–7].

However, since the (112) surface normal of TaAs deviates from a high symmetry axis (e.g. the a and c axes) of the tetragonal unit cell, the excitation of shear acoustic waves becomes possible [5, 7]. Here, photoinduced stress drives both quasi-longitudinal (QL) and quasi-shear (QS)

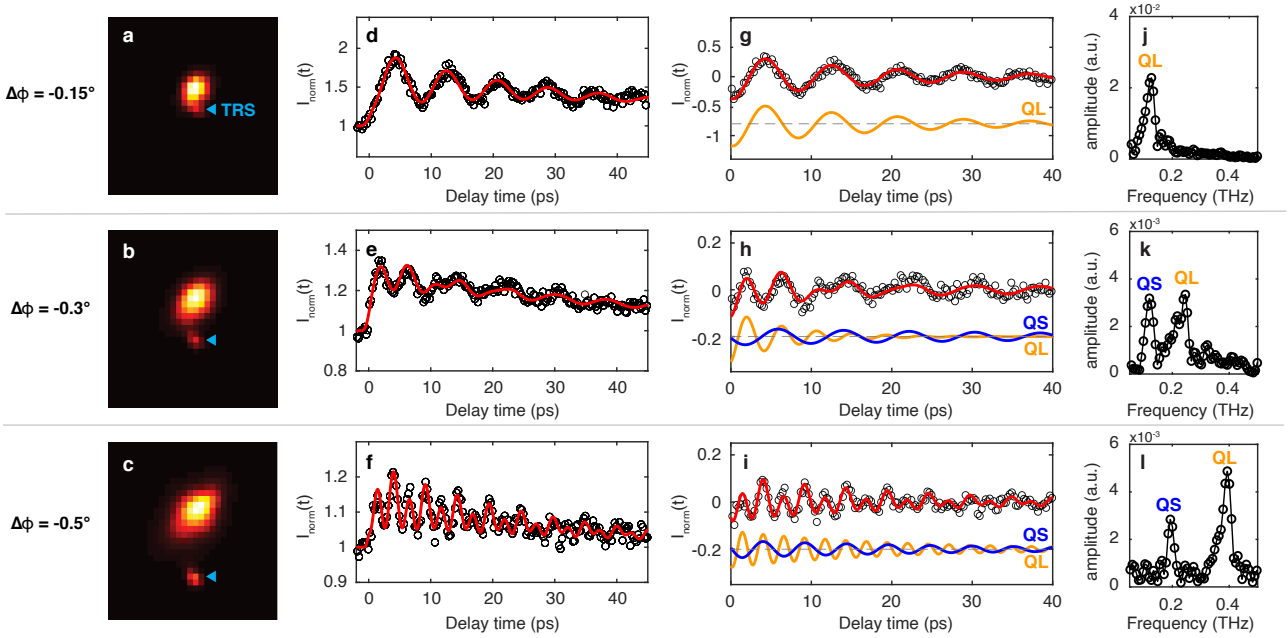

FIG. 2. (a-c) Two-dimensional XRD images, showing diffuse scattering and TRS signals without pump excitation. Here, variation of the azimuthal angle, $\Delta\phi$, enables the TRS peak (blue arrow) to be resolved. (d-f) Time-resolved traces of the TRS signal, integrated over the 3 x 3 pixel area of the detector indicated by the blue arrow, reveal clear coherent acoustic phonon oscillations. These oscillations were isolated and extracted from (d-f) for azimuthal angles of $\Delta\phi =$ (g) $-0.15°$, (h) $-0.3°$, and (i) $-0.5°$, along with their spectral amplitudes (j-l). Experimental data (open symbols) was fit (solid red lines) as described in the text, where the separate fit components for quasi-longitudinal (QL-solid orange lines) and quasi-shear (QS-solid blue lines) modes are shown below.

acoustic modes, with displacements that are not purely longitudinal or transverse to the (112) axis. While the generation of shear modes is often forbidden by crystal symmetry, choice of a miscut or reduced symmetry face supports the excitation of these modes [5–7, 28–32]. Furthermore, by using an X-ray probe, we can trace the dispersion of coherently excited acoustic modes by changing the scattering geometry (as shown in Eq. (1)) [16, 22], a significant advantage over optical experiments [8]. Recent tr-XRD studies did observe shear strain in molecular films and multiferroic oxides [29, 30], but they only focused on Bragg peaks, not the TRS signal, preventing them from measuring the phonon dispersion.

A comparison between first principles calculations and the experimentally determined acoustic phonon dispersion along the Γ (000) to (112) direction near the Brillouin zone center is shown in Fig. 3 as a function of phonon momentum q (defined in Eq. (1) [27]). Here, the calculated dispersion (Fig. 3(a)) reveals three acoustic branches that are attributed to a single longitudinal acoustic (LA) mode and two transverse acoustic (TA) modes. This agrees well with the experimentally determined q-dependence of the QL and QS modes obtained from our tr-XRD measurements, as shown in Fig. 3(b). For more insight into the origin of these modes, we used the elastic modulus tensor [27] to calculate the phonon polarization. This shows that the atomic vibrations of the LA mode predominately align along the (112) surface normal, with an angular deviation of 7.5° with respect to this axis (Fig. 3(c)). Similarly, the higher-frequency TA mode (TA2) is nearly orthogonal to the (112) normal, deviating by 82.5° with respect to this direction. In addition, we note that only one TA mode (TA2) was observed in our experiments, as the other (TA1) is polarized along the $(1\bar{1}0)$ axis, which makes it orthogonal to the sagittal $(1\bar{1}0)$ plane and therefore invisible in our TRS experiments, because thermoelastic expansion cannot excite this TA1 mode with respect to this mirror-symmetric plane. This knowledge of the phonon polarization and comparison to our first principles calculations allows us to conclude that the observed QL and QS modes are the LA and TA2 modes, respectively, in TaAs.

Closer examination of the QL mode in Fig. 2(j-l) reveals an asymmetric spectral lineshape, which contrasts strongly with the symmetric lineshape of the QS mode [27]. Previous studies on transition metal monopnictide Weyl semimetals revealed strong electron-phonon coupling, as inferred from the asymmetric Fano lineshape fitting both Raman-active [33] and infrared-active [34] optical phonons. We therefore considered a similar mechanism for the QL mode, but found that a Fano lineshape failed to capture the observed asymmetry (Fig. 4) [35], consistent with the weak phonon renormalization present for the LA and TA modes near the Brillouin zone cen-

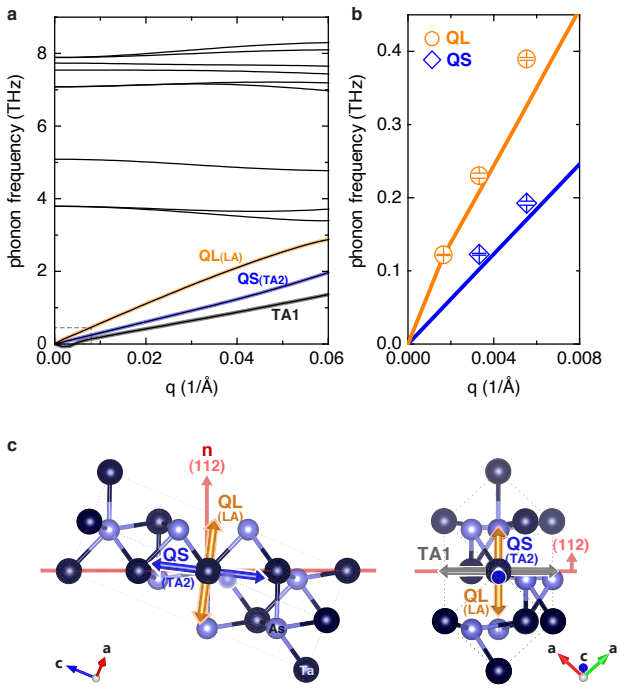

FIG. 3. (a) Calculated phonon dispersion along the (112) direction in TaAs, with the LA (orange), TA2 (blue), and TA1 (grey) modes clearly indicated. (b) Comparison of calculated (lines) and experimentally determined (open symbols) acoustic phonon dispersion measured near the Brillouin zone center (000). Here, quasi-longitudinal (QL) and quasi-shear (QS) modes are indicated in orange and blue, respectively. (c) Schematic diagram illustrating the polarization of the QL (LA, orange), QS (TA2, blue), and TA1 (grey) modes with respect to the wavevector along the (112) normal. The (112) and (1$\bar{1}$0) planes are also displayed in red and black, respectively.

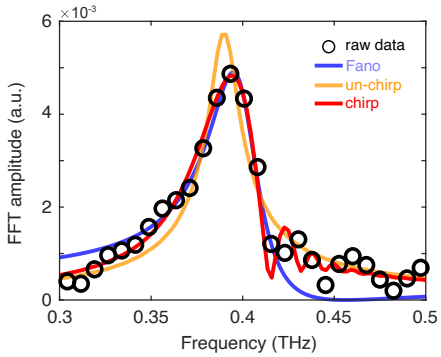

FIG. 4. Fits (solid lines) to the spectral lineshape of the QL mode (open circles) for $\Delta\phi = -0.5^\circ$ using Fano resonance (blue), time-invariant (un-chirped frequency)(orange), and time-variant (positive frequency chirp)(red) frequency models.

ter [33]. This suggests an alternative mechanism governing the asymmetry in the QL phonon lineshape, based on a small ($< 4\%$) time-dependent frequency chirp. In fact, we found that a linearly increasing, time-varying frequency given by $f(t) = f_0'(1+Ct)$, valid for early time delays ($t \sim \leq 40$ ps), reproduces well the asymmetric spectral lineshape of the QL mode for $C = 1$ ns^{-1} with minimum deviation from our data, in contrast with fits based on a time-invariant frequency f_0 (Fig. 4). Such a positive frequency chirp is also supported by time-dependent Fourier transform and frequency data (Fig. S4), and fits our data over the entire q-dependence of the QL mode ($\Delta\phi = -0.15^\circ$ and -0.3°) with a constant value of the chirp coefficient C (Fig. S5), demonstrating this effect to be independent of phonon momentum [27].

Microscopically, such a positive frequency chirp has been observed using picosecond ultrasonics, in which a broadband strain pulse, injected by impulsive optical excitation, spreads in both time and space through the effect of phonon dispersion, but does not produce an asymmetric lineshape [36, 37]. Instead, the positive frequency chirp and asymmetric lineshape of the QL mode may be linked to the ambipolar diffusion of photoinduced carriers [38]. We estimate that these carriers diffuse into the sample over a distance of $\sim$100 nm [39], much larger than the penetration depth of the optical pump (22 nm), but within our X-ray probing depth (500 nm). The resulting carrier density gradient could influence the observed frequency chirp by changing the electronic structure and total energy of the system, which would in turn modify interatomic forces and cause phonon softening [43]. This would initially reduce the frequency of the QL mode, which would then increase as the acoustic wave propagates deeper into the sample, leading to the observed frequency chirp. Alternatively, the photoinduced carrier density gradient would also create a thermal gradient along the surface normal (via electron-phonon thermalization) [44]. This could soften the QL mode near the surface, which then would become progressively harder as the strain wave propagates down the thermal gradient to cooler regions of the crystal. In contrast, the symmetric lineshape of the QS mode is likely due to the fact that the shear velocity may be less sensitive to carrier diffusion or temperature [45, 46] than its longitudinal counterpart.

To the best of our knowledge, this is the first observation of a frequency chirp in coherent acoustic phonon oscillations from any material using ultrafast X-ray diffraction, as previous tr-XRD studies did not observe this effect [16, 21, 22, 29, 30]. Here, the large X-ray penetration depth and high time resolution of our experiments enabled us to capture the time-dependent variation in the phonon frequency. Finally, we note that this is a general phenomenon that should occur in most conducting materials due to fast photocarrier diffusion [47]; our observation thus underlines the advantages of X-ray probes for probing condensed matter.

In conclusion, we investigated the coherent excitation of acoustic phonons in TaAs following femtosecond optical excitation. Due to the distinct crystallographic orientation of the (112) surface probed in our experiment, both longitudinal and transverse acoustic modes were excited. Our calculations demonstrated that the QL mode is polarized nearly parallel to the (112) normal, while the QS mode is necessarily perpendicular to this direction. We also observed an asymmetry in the spectral lineshape of the QL mode, which we attribute to a phonon frequency chirp arising from the ambipolar diffusion of photoinduced carriers on ultrafast timescales.

More generally, the use of off-axis crystal orientations to optically excite shear deformations in topological semimetals offers a promising route for transiently altering structural and thus topological properties in these materials. This is especially relevant, as shear strain induced by ultrafast THz excitation has been shown to induce symmetry changes in Dirac [11, 12] and Weyl semimetals [13], making these materials amenable for use as topological transistors. Through the choice of an off-axis crystal orientation, the generation of shear strain follows directly from optical excitation through a generic, thermoelastic processes, rather than a direct piezoelectric effect brought on by THz pulses. This then offers a promising avenue for inducing shear deformations for breaking or restoring symmetry in these topological semimetals on ultrashort timescales.

This work was performed at the Center for Integrated Nanotechnologies at Los Alamos National Laboratory (LANL), a U.S. Department of Energy, Office of Basic Energy Sciences user facility, under user proposal 2018BU0083. It was primarily supported through the U.S. Department of Energy, Office of Science, Office of Basic Energy Sciences, Division of Materials Sciences and Engineering via FWP No. 2018LANLBES16 (M.-C. L. and R. P. P.), Contract No. DE-AC02-76SF00515 (S. T., V. K., Y. H., M. T. and D. A. R.) and Contract No. DE-SC0019126 (A. M., T. P., J. S. and K. A. N.). Use of the LCLS is supported by the U.S. Department of Energy, Office of Science, Office of Basic Energy Sciences under Contract No. DE-AC02-76SF00515. J.-X. Z., and D. A. Y. are supported by the Center for Advancement of Topological Semimetals, an Energy Frontier Research Center funded by the U.S. Department of Energy Office of Science, Office of Basic Energy Sciences, through the Ames Laboratory under its Contract No. DE-AC02-07CH11358. N. S. was supported by the LANL LDRD program. This research used resources at the National Energy Research Scientific Computing Center (NERSC), a U.S. Department of Energy Office of Science User Facility operated under Contract No. DE-AC02-05CH11231. We appreciate Matthieu Chollets assistance in performing experiments at the LCLS XPP beamline.

* Corresponding author; mclee@lanl.gov
† Corresponding author; rpprasan@lanl.gov

[1] H. J. Zeiger, J. Vidal, T. K. Cheng, E. P. Ippen, G. Dresselhaus, and M. S. Dresselhaus, Phys. Rev. B **45**, 768 (1992).
[2] L. Dhar, J. A. Rogers, and K. A. Nelson, Chem. Rev. **94**, 157 (1994).
[3] M.-C. Lee *et al.*, Phys. Rev. B **99**, 144306 (2019).
[4] C. Thomsen, H. T. Grahn, H. J. Maris, and J. Tauc, Phys. Rev. B **34**, 4129 (1986).
[5] T. Pezeril, Opt. Laser Technol. **83**, 177 (2016).
[6] O. Matsuda, O. B. Wright, D. H. Hurley, V. E. Gusev, and K. Shimizu, Phys. Rev. Lett. **93**, 095501 (2004).
[7] T. Pezeril, P. Ruello, S. Gougeon, N. Chigarev, D. Mounier, J.-M. Breteau, P. Picart, and V. Gusev, Phys. Rev. B **75**, 174307 (2007).
[8] D. A. Reis and A. M. Lindenberg, in Light Scattering in Solids IX, edited by M. Cardona and R. Merlin (Springer-Verlag, Berlin, 2007), p. 371.
[9] J. Lee, S. A. Trugman, C. L. Zhang, D. Talbayev, X. S. Xu, S.-W. Cheong, D. A. Yarotski, A. J. Talyor, and R. P. Prasankumar, Appl. Phys. Lett. **107**, 042906 (2015).
[10] P. Ruello and V. E. Gusev, Ultrasonics **56**, 21 (2015).
[11] J. Mutch, W.-C. Chen, P. Went, T. Qian, I. Z. Wilson, A. Andreev, C.-C. Chen, J.-H. Chu, Sci. Adv. **5**, eaav9771 (2019).
[12] C. Vaswani, L.-L. Wang, D. H. Mudiyanselage, Q. Li, P. M. Lozano, G. D. Gu, *et al.*, Phys. Rev. X **10**, 021013 (2020).
[13] E.J. Sie, *et al.*, Nature **565**, 61 (2019).
[14] C. Bostedt *et al.*, Rev. Mod. Phys. **88**, 015007 (2016).
[15] C. Dornes *et al.*, Nature **565**, 209 (2019).
[16] T. Henighan, M. Trigo, S. Bonetti, P. Granitzka, D. Higley, Z. Chen *et al.*, Phys. Rev. B **93**, 220301(R) (2016).
[17] M. Bargheer, N. Zhavoronkov, Y. Gritsai, J. C. Woo, D.-S. Kim, M. W?rner, and T. Els?sser, Science **306**, 1771 (2004).
[18] A. A. Maznev, K. J. Manke, K.-H. Lin, K. A. Nelson, C.-K. Sun, and J.-I. Chyi, Ultrasonics **52**, 1 (2012).
[19] R. Legrand, A. Huynh, B. Jusserand, B. Perrin, and A. Lemaitre, Phys. Rev. B **93**, 184304 (2016).
[20] T.-H. Chou, L. Lindsay, A. A. Maznev, J. S. Gandhi, D. W. Stokes, R. L. Forrest, A. Bensaoula, K. A. Nelson, and C.-K. Sun, Phys. Rev. B **100**, 094302 (2019).
[21] D. A. Reis *et al*, Phys. Rev. Lett. **86**, 3072 (2001).
[22] A. M. Lindenberg *et al.*, Phys. Rev. Lett. **84**, 111 (2000).
[23] G. Blaj *et al.*, J. Synchrotron Radiat. **22**, 577 (2015).
[24] G.S. Saini, L. D. Calvert, and J. B. Taylor, Can. J. Chem. **42**, 630 (1964).
[25] B. Q. Lv *et al.*, Phys. Rev. X **5**, 031013 (2015).
[26] I. K. Robinson, Phys. Rev. B **33**, 3830 (1986).
[27] See the supplementary material for additional experimental and theoretical details.
[28] We note that recent time-resolved X-ray diffraction experiments also simultaneously observed both longitudinal and shear acoustic waves [15], in which the shear mode is driven by a magnetic effect with external fields since the surface normal is oriented along a high symmetry axis (and shear mode generation is normally not allowed).
[29] H. T. Lemke *et al.*, ACS Omega **3**, 9929 (2018).

[30] V. Juvé *et al.*, arXiv:2007.10967v1

[31] P. Ruello, T. Pezeril, S. Avanesyan, G. Vaudel, V. Gusev, I. C. Infante, and B. Dkhil, Appl. Phys. Lett. **100**, 212906 (2012).

[32] M. Lejman, G. Vaudel, I. C. Infante, P. Gemeiner, V. E. Gusev, B. Dkhil, and P. Ruello, Nat. Commun. **5**, 4301 (2014).

[33] J. Coulter, G. B. Osterhoudt, C. A. C. Garcia, Y. Wang, V. M. Plisson, B. Shen, N. Ni, K. S. Burch, and P. Narang, Phys. Rev. B **100**, 220301(R) (2019).

[34] B. Xu *et al.*, Nat. Commun. **8**, 14933 (2017).

[35] U. Fano, Phys. Rev. **124**, 1866 (1961).

[36] H.-Y. Hao and H. J. Maris, Phys. Rev. Lett. **84**, 5556 (2000).

[37] C. L. Poyser, W. B. York, D. Srikanthreddy, B. A. Glavin, T. L. Linnik, R. P. Campion, A. V. Akimov, and A. J. Kent, Phys. Rev. Lett. **119**, 255502 (2017).

[38] B. A. Ruzicka, L. K. Werake, H. Samassekou, and H. Zhao, Appl. Phys. Lett. **97**, 262119 (2010).

[39] Using the Einstein relation of diffusivity [40], we can estimate the ambipolar diffusivity: $D_e = \mu k_B T/e$, where μ, k_B, T, and e are the mobility, Boltzmann constant, temperature, and electron charge, respectively. With $\mu = 3000$ cm^{2}V^{1}s^{-1} at $T = 300$ K [41] and the scattering time via electron-phonon coupling $\tau = 1.1$ ps [42], we obtain $D_e = 77.6$ cm^2/s, resulting in the diffusion length of $l = \sqrt{D_e \tau} = 92.4$ nm.

[40] L. D. Landau, E. M. Lifshitz, and L. P. Pitaevskii, Electrodynamics of Continuous Media (ButterworthHeinemann, Oxford, 1984), Chap. III.

[41] C.-L. Zhang *et al*, Nat. Commun. **7**, 10735 (2016).

[42] C. P. Weber *et al.*, J. Appl. Phys. **122**, 223102 (2017).

[43] S. W. Teitelbaum *et al.*, arXiv:1908.07161.

[44] I. Chaban, H. D. Shin, C. Klieber, R. Busselez, V. E. Gusev, K. A. Nelson, and T. Pezeril, Rev. Sci. Instrum. **88**, 074904 (2017).

[45] A. Timur, Geophysics **42**, 950 (1977).

[46] C. Klieber, T. Hecksher, T. Pezeril, D. H. Torchinsky, J. C. Dyre, and Keith A. Nelson, J. Chem. Phys. **138**, 12A544 (2013).

[47] M. F. DeCamp *et al.*, Phys. Rev. Lett. **91**, 165502 (2003).